

Derivation of Response Spectra and Hysteretic Energy: A Case Study on 2023 Turkey-Syria Earthquake in Consideration of Structural Ductility



Weiye Shao

Abstract Structural response under strong ground motion has always been of concern in engineering seismology due to low predictability of seismic events and their devastating impact. The energy-based seismic design (EBSD) is proposed to capture the cumulative damage of the structure in terms of evaluating hysteretic energy, which is a more reasonable design method considering inelastic deformation of structures. On the other hand, structural ductility demand is another significant aspect of design. In this paper, the response spectra and hysteretic energy under different ductility factors are derived and quantified based on a selection of ground motion records from the recent 2023 Turkey-Syria earthquake mainshock (M7.7) and aftershock (M7.6). The results show that for the selected data, the peak value of acceleration response spectra significantly exceeds the design acceleration, and the hysteretic energy for M7.7 presents a relatively high value while the value for M7.6 is comparatively lower. Even if the evaluation for the M7.6 event is minor, it is worth considering the structural vulnerability under cumulative damage and residual influence from the mainshock.

Keywords Response spectra · Hysteretic energy · Energy-based seismic design · Structural ductility · Single-degree-of-freedom system

1 Introduction

Structural response under strong ground motion is acknowledged as one of the most significant issues in engineering seismology due to the low predictability of seismic events and their destructive impact on structures. The mainstream of structural reliability and performance assessment is probabilistic seismic hazard analysis (PSHA), which is extensively used as method for potential damage estimation under earthquakes, and its efficiency and accuracy have been proved over the past few decades

W. Shao (✉)
University of Bristol, Bristol BS8 1TR, UK
e-mail: ql21598@alumni.bristol.ac.uk

© The Author(s), under exclusive license to Springer Nature Singapore Pte Ltd. 2024
M. Casini (ed.), *Proceedings of the 3rd International Civil Engineering and Architecture Conference*, Lecture Notes in Civil Engineering 389,
https://doi.org/10.1007/978-981-99-6368-3_34

399

[1]. The dedication that has been devoted to this topic is prominent, and the works of performing simulation on models, creating design spectra and hazard maps based on specific events have improved the seismic risk assessment at design stage as well as in post-hazard investigation.

On the one hand, the code-based seismic design mainly targets on elastic response of structures. For instance, force-based seismic design and displacement-based design, which are the most commonly used method for earthquake-resistant structural design [2, 3]. However, it has been conventionally acknowledged that structures not only suffer from elastic displacement under ground motion, but also experience inelastic hysteretic deformation which is closely associated with energy-based seismic design (EBS) [2, 4]. The application of EBS which takes the impact of cumulative damage into account in design codes is less prevalent, but has gradually been adopted in seismic design and risk assessment, and this design method can better predict the structural response compared with ordinary code-based seismic design under some circumstances, where the energy spectra present distinctive peak response while the spectral acceleration would probably fail to capture [4].

From seismic input energy perspective, the total input seismic energy can be classified into recoverable energy and dissipated energy, while recoverable energy consists of elastic strain energy and kinetic energy, and dissipated energy can be further classified into damping energy and hysteretic energy [2, 4]. The hysteretic energy, in particular, is related to the inelastic behavior that may cause permanent damage to the structure. Consequently, in EBS, the priority of design resides in the overall hysteretic energy demand and corresponding inelastic deformation [2].

On the other hand, structural damage is correlated with ductility demand, and it is stressed in seismic design codes that the ductility demand is vital in seismic-prone regions; therefore, the investigation of desired ductility level of structures resisting strong ground motion is critical [5]. Hatzigeorgiou evaluates the ductility demand of single-degree-of-freedom (SDOF) systems under multiple near-fault and far-fault earthquakes, and it has been concluded that the design earthquake is insufficient to estimate structural performance under real earthquake sequences [5]. Therefore, as a complementary aspect, the hysteretic energy for different structural ductility under real earthquake records can provide a better quantification of seismic demand.

In general, this paper presents the conventional response spectra and the estimation of hysteretic energy for SDOF system of the recent Turkey-Syria earthquake (2023) in order to quantify the difference between the code-based seismic design and EBS. In Sect. 2, a brief introduction of this seismic event is stated, and the formulation of calculating hysteretic energy as well as the selection of ground motion records is clarified in Sect. 3. The result is discussed in Sect. 4 in order to compare the acceleration spectra and hysteretic energy for different categories. Finally, conclusions are drawn in Sect. 5 based on the results obtained, the scope of the analysis and proposal of future research directions.

2 Case-Study Event: 2023 Turkey-Syria Earthquake

On February 6th, 2023, a strong earthquake with magnitude 7.8 (M7.7 for AFAD inspection) struck south-eastern Turkey with thousands of aftershock sequences, influencing north-western Syria as well [6]. According to the engineering report and Turkish database AFAD, the earthquake is featured with 3 major events: first and mainshock with Mw of 7.7 (01:17 UTC), second event which happened closely after the mainshock with Mw of 6.6 (01:28 UTC) and another unexpected strong aftershock happened within 12 h with Mw of 7.6 (10:24 UTC) [6, 7]. All of them are caused by strike-slip mechanism. The epicentre of the M7.7 earthquake is 37.288°N, 37.043°E with a depth of 8.6 km, while for the M7.6 earthquake, the epicentre is around 10 km away with depth of 7 km (38.089°N, 37.239°E) [7].

Despite that it is suggested to evaluate the impact of the second M6.6 earthquake, the main analysis relies on the first M7.7 and the third M7.6 ground motion. Nevertheless, the acceleration time-histories of the M7.7 and the M6.6 earthquakes for station 2708 (37.099°N, 36.648°E) are illustrated in Fig. 1. For each ground motion, the station recorded the data in 3 directions: east-west (EW), north-south (NS) and up-down (UD). For the M7.7 earthquake, the peak ground acceleration (PGA) values reach 0.93, 1.32, and 0.69 g for the three components respectively, but for M6.6 event, the PGA value is lower (0.36, 0.32, and 0.22 g). However, the latest 2019 Turkish earthquake code TEC 19 indicates design acceleration at 0.3 g, and it is unreasonable to design structures at high acceleration level even in earthquake-prone region [8]. As a result, the impact on structure is severe, including demolition of buildings, inundation in coastal area and small tsunamis [9, 10].

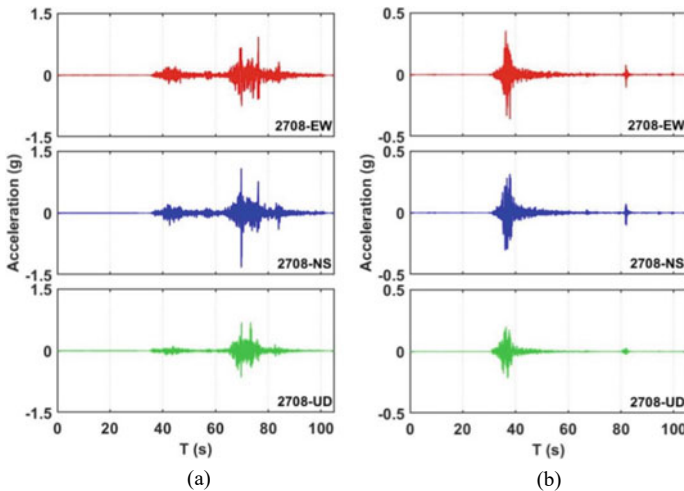


Fig. 1. Acceleration time-history at Station 2708 (37.099°E, 36.648°N): **a** Mw 7.7, 01:17 (UTC) and **b** Mw 6.6, 01:28 (UTC)

3 Methodology

3.1 Estimation of Seismic Input Energy and Hysteretic Energy

The first theoretical identification of seismic energy concept is proposed by Housner [11], followed by several studies on analysis of SDOF systems evaluating the damage from energy perspective (e.g. Akiyama (1985), Fajfar and Vidic (1994)) [12, 13]. The formulation that has been used in this paper to estimate the total input and hysteretic energy is proposed by Khashae (2004) [14]. For the total input seismic energy EI per unit mass m, the formulation is shown as Eq. 1:

$$\frac{E_I}{m} = \bar{f} \cdot f_T \cdot \frac{1}{2} \cdot \left(\frac{Sa}{\omega} \right)^2 \quad (1)$$

where $\frac{Sa}{\omega}$ is the pseudo-spectral velocity (evaluated with 5% damping ratio), \bar{f} and f_T can be calculated as follow (Eq. 2–3):

$$\begin{cases} f_T = 0.572e^{(-4.283T_n)} + 0.6 \text{ for } \mu = 1 \\ f_T = 1 \text{ for } \mu = 2, 3, 4, 5 \end{cases} \quad (2)$$

$$\bar{f} = \frac{4.256}{\sqrt{\mu - 0.5}} + 0.318I_c \quad (3)$$

where μ is the ductility of structure, and I_c is the intensity index which can be calculated as Eq. 4:

$$I_c = (a_{rms})^{1.5} (t_{di})^{0.5} \quad (4)$$

where a_{rms} is the root-mean square ground acceleration and t_{di} is the 5–95% duration of strong motion (Eq. 5–6).

$$a_{rms} = \left(\frac{1}{T_2 - T_1} \cdot \int_{T_1}^{T_2} [a(t)]^2 dt \right)^{0.5} \quad (5)$$

$$t_{di} = T_{0.95} - T_{0.05} \quad (6)$$

Eventually, the hysteretic energy E_H can be evaluated as Eq. 7:

$$\begin{cases} E_H = 0 \text{ for } \mu = 1 \\ E_H = 0.72(1 - \mu^{-1})^{0.7} E_I \text{ for } \mu = 2, 3, 4, 5 \end{cases} \quad (7)$$

The benefit of these formulae is the efficiency and accuracy of predicting input and hysteretic energy based on regression analysis of 160 accelerograms, and it does not involve the cyclic ductility variable [14].

3.2 Selection of Ground Motion Records

The selection of ground motions was made based on the nearest stations for each event listed in preliminary engineering report, and corresponding acceleration time-history was available on AFAD [6, 7]. For the mainshock (M7.7) and aftershock (M7.6), 20 records are selected from the database respectively in terms of source-to-site distance and availability of record data to proceed further analysis. The basic information of the stations is shown in Table 1.

Table 1 Selected stations and basic information (adapted from Baltzopoulos et al. [6])

M7.7, 01:17 (UTC)			M7.6, 10:24 (UTC)		
Station No	V_{S30} (m/s) / EC8 Ground type	R_{epi} (km)	Station No	V_{S30} (m/s) / EC8 Ground type	R_{epi} (km)
0201	391 (B)	120.12	0129	965 (A)	91.84
2703	758 (A)	37.34	0141	/	161.28
2704	721 (B)	74.10	0213	/	68.73
2708	523 (B)	40.77	3802	305 (C)	77.41
2709	555 (B) 90	37.45	3803	499 (C)	157.41
2712	/	29.79	3804	637 (B)	102.93
3123	470 (B)	143.00	4405	579 (B)	100.81
3125	448 (B)	142.15	4406	815 (A)	70.17
3126	350 (C)	143.54	4408	654 (B)	56.74
3129	447 (B)	146.39	4409	/	56.86
3135	460 (B)	142.15	4410	/	94.59
3137	688 (B)	82.48	4412	/	99.89 99.89 99.89
3141	338 (C)	125.42	4611	731 (B)	38.21
3142	539 (B)	106.49	4612	246 (C)	66.68
4615	484 (B)	13.83	4614	671 (B)	67.35
4616	390 (B)	20.54	4617	574 (B)	66.50
4629	382 (B)	22.50	4620	484 (B)	63.46
4630	347 (C)	21.89	4628	186 (C)	32.41
4632	428 (B)	24.09	4631	543 (B)	21.43
NAR	/	15.35	5807	445 (B)	70.94

4 Results and Analysis

4.1 Response Spectra

The response spectra are illustrated in Fig. 2 for M7.7 and M7.6 event, and each component, respectively. The preliminary acceleration time-history was downloaded from AFAD [8], and processed in MATLAB [15] and SeismoSignal [16]. It should be noted that the damping ratio ζ equals to 5% as it is generally defined in pseudo-spectral acceleration (PSA) calculation. For PSA spectra, the mean value as well as plus/minus one standard deviation is evaluated for each event and component in order to assess central tendency as well as the variability and significance range of each sample.

From Fig. 2a, c, and e, it can be observed that the mean value and plus/minus standard deviation is similar for EW and NS with maximum mean value of 1.42 and 1.54 g, but relatively lower for UD especially after $T = 0.3$ s, where the mean value of UD only presents half of the mean value for EW and NS. This minor PSA value indicates less significance of acceleration in UD direction compared with EW and NS component, however, the peak mean value for UD still reaches 1.18 g which is far more notable with respect to the design acceleration level (0.3 g).

The comparison between Fig. 2a–f is made, and the differences between two events are prominent. Even though the mean value and plus/minus standard deviation falls beneath 0.4 g, the maximum value of sample mean for EW (0.32 g) and NS (0.29 g) is close to design acceleration. In addition, the damage that structures suffered from the mainshock is not negligible, which suggests that the structures are much more vulnerable when experiencing this strong aftershock. As a result, the impact of the spectral acceleration for M7.6 is also pronounced and destructive.

4.2 Hysteretic Energy

Having the PSA values, the mean value and plus/minus standard deviation of hysteretic energy per unit mass (E_H/m) for each ductility category ($\mu = 2, 3, 4$ and 5) is derived using the equations mentioned in Sect. 3.1.

The results are shown in Fig. 3, where for both two events NS component presents higher average hysteretic energy than EW and UD, and M7.7 event apparently possesses larger hysteretic energy for all of the components. The maximum value of mean for M7.7 usually appears within the period range of $T = 1.0$ – 2.3 s, but for M7.6 this range as well as the variability range is narrower ($T = 1.3$ – 1.7 s). Specifically, for UD component of M7.7 and M7.6, the peak falls in $T = 2.0$ – 3.0 s, and its value is excessively lower than EW and NS. In terms of different ductility level of SDOF systems, lower ductility presents higher hysteretic energy under most of the scenarios, however, for M7.7 EW and NS (Fig. 3a, c), the most distinct hysteretic

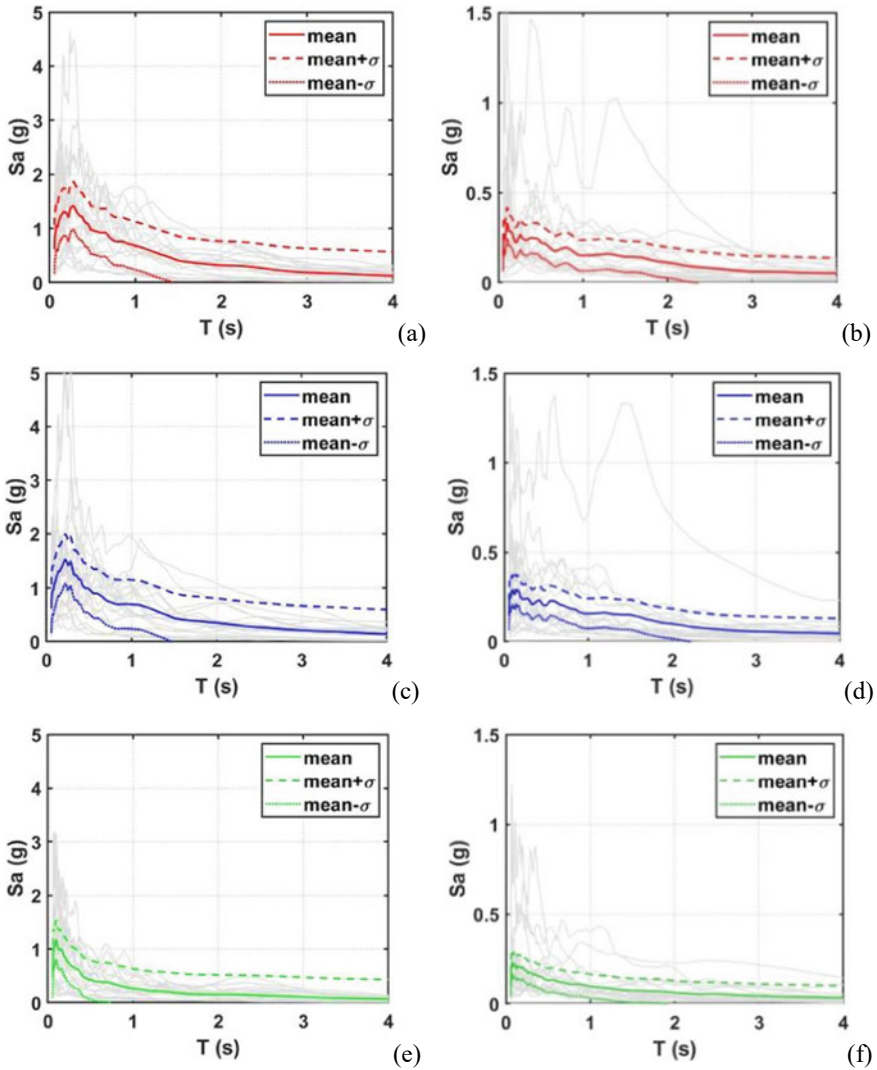


Fig. 2 Response spectra (acceleration) ($\zeta = 5\%$) for: **a** M7.7, EW; **b** M7.6, EW; **c** M7.7, NS; **d** M7.6, NS; **e** M7.7, UD and **f** M7.6, UD

energy is observed in $\mu = 3$ rather than $\mu = 2$. It is true as the ductility level indicates the ability of structures withstanding large displacement under strong ground motions, and also the ability to dissipate seismic energy during an earthquake. Consequently, a higher ductility level usually suggests better performance. However, for SDOF systems under actual scenario, the overall stiffness would be higher than MDOF systems using the same material, so the ductility level is more essential to

prevent brittle structures. With a certain capacity of deformation defined by structural ductility, the energy dissipation is in direct proportion to ductility, so it is more profitable to improve the ductility to achieve better energy dissipation.

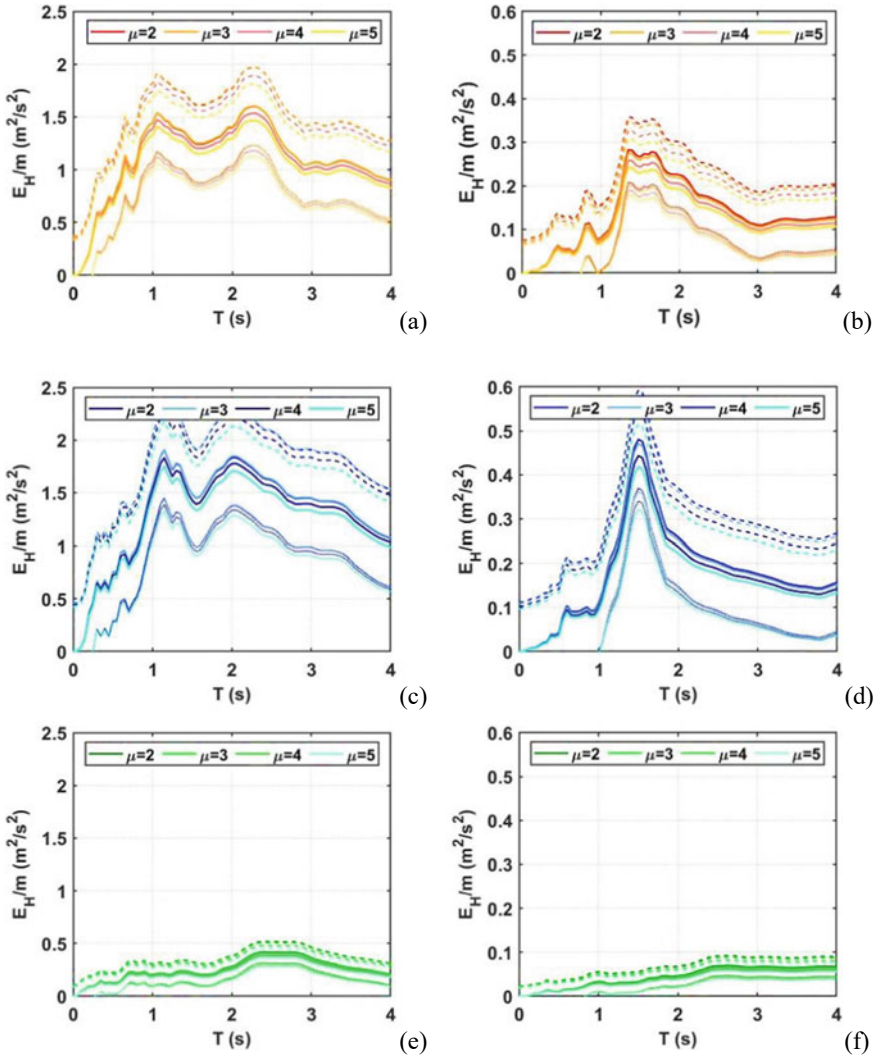


Fig. 3 Hysteretic energy spectra for SDOF systems with different ductility μ ($\zeta = 5\%$): **a** M7.7, EW; **b** M7.6, EW; **c** M7.7, NS; **d** M7.6, NS; **e** M7.7, UD and **f** M7.6, UD

5 Conclusion

In this paper, general information on EBSD and empirical formulation on hysteretic energy estimation as well as geotechnical details of 2023 Turkey-Syria earthquake is introduced. PSA and E_H/m are chosen as intensity measures to describe M7.7 and M7.6 events. The implementation of response spectra shows an excessive high maximum value of average PSA for M7.7 (1.42, 1.54, and 1.18 g for EW, NS and UD) compared with design level (0.3 g), and the maximum value of average PSA reaches design acceleration for M7.6 (0.32, 0.29, and 0.24 g for EW, NS and UD). However, the residual effect of the mainshock should be taken into account when evaluating the second major aftershock M7.6 for potential damage and vulnerability (e.g. interior cracking) of structures.

In terms of hysteretic energy, higher energy level is observed in NS component, while the M7.7 earthquake presents larger hysteretic demand than M7.6 earthquake. The peak value of average E_H/m depends on the event and component, for UD shows late peak value which falls in medium-to-long period ($T = 2.0-3.0$ s), and the period range in which peak value appears for M7.6 ($T = 1.3-1.7$ s) event is more concentrated than M7.7 ($T = 1.0-2.3$ s). The overall tendency of ductility-related analysis on SDOF systems is as expected, for the hysteretic energy decreased as ductility increased for most of the cases except for some individual cases, in which distinction is subtle to be visualized between $\mu = 2$ and $\mu = 3$.

Even though the study is carried out based on the formulation with great accuracy and efficiency of predicting input and hysteretic energy based on regression analysis of 160 accelerograms without the requirement of considering cyclic ductility variables, a comparison between total input and hysteretic energy expression proposed by different scholars and the real earthquake scenario was made, and the results indicated that the ratio of hysteretic energy over input seismic energy generally overestimates the real energy demand [2]. However, conservative prediction is necessary in determining structural response, for rationally raised seismic demand can better ensure the safety of structures under ground motions which are extremely intensive.

Despite the fact that the consistency between the data obtained from PSHA and the actual response caused by real earthquakes is controversial, it is comparatively reliable if the derivation and assessment process has taken various factors into consideration (e.g. site condition, geotechnical and rupture mechanism, etc.) [17]. For further work orientation, the selection of 20 records for each event is insufficient due to the deficiency of stations, unavailability of records and limitation of database. Therefore, a more extensive selection of ground motion records should be made and data that shows low consistency should be eliminated. Moreover, the pulse-like ground motions can cause more severe damage to structures than ordinary records, and the identification of pulse-like content in this seismic event has been carried out [18]. Further investigation into the influence of pulse-like records on different structural systems should be simulated and evaluated, and the potential inadequacy of the model or analysis should be discussed.

References

1. Mulargia F, Stark PB, Geller RJ (2017) Why is probabilistic seismic hazard analysis (PSHA) still used? *Phys Earth Planetar Inter* 264:63–75, ISSN 0031–9201. <https://doi.org/10.1016/j.pepi.2016.12.002>
2. Mezgebo MG (2015) Estimation of Earthquake Input Energy, Hysteretic Energy and its Distribution in MDOF Structures”. Dissertations—ALL, pp 228. Retrieved from <https://surface.syr.edu/etd/228>
3. Eurocode 8 (2004) Design of structures for earthquake resistance. British Standards Institution, London: BSI
4. Ying Z, Ge S, Ping T (2019) Hysteretic energy demand for self-centering SDOF systems. *Soil Dynam Earthquake Eng* 125:105703, ISSN 0267–7261. <https://doi.org/10.1016/j.soildyn.2019.105703>
5. Hatzigeorgiou GD (2010) Ductility demand spectra for multiple near- and far-fault earthquakes. *Soil Dynam Earthquake Eng* 30(4):170–183, ISSN 0267–7261, <https://doi.org/10.1016/j.soildyn.2009.10.003>
6. Baltzopoulos G, Baraschino R, Chioccarelli E, Cito P, Iervolino I (2023) Preliminary engineering report on ground motion data of the Feb. 2023 Turkey seismic sequence V2.0—10/02/2023. <https://doi.org/10.13140/RG.2.2.31375.25767>
7. Ground motion records AFAD. Retrieved from <https://tadas.afad.gov.tr/list-waveform>. Accessed 20/02/2023 9:35 UTC
8. AFAD (2019) The disaster and emergency management authority of Turkey. “Turkish Building Earthquake Code, TEC 19”
9. Ravilius K (2023) Geological impact of Turkey-Syria earthquake slowly comes into focus. *The Guardian*
10. Damaskinos I (2023) Earthquake in Turkey caused ‘small tsunamis’ off Famagusta coast. *Cyprus Mail*. Archived from the original on 6 February 2023. Accessed on February 2023
11. Housner GW (1956) Limit design of structures to resist earthquakes. In: Proceedings of the first world conference on earthquake engineering, EERI, Berkeley, CA
12. Akiyama H (1985) Earthquake-resistant limit state design for building. University of Tokyo Press, Tokyo
13. Fajfar P, Vidic T (1994) Consistent inelastic design spectra: hysteretic and input energy. *Earthquake Eng Struct Dynam* 23:523–537
14. Khashaee (2004) Energy-based seismic design and damage assessment for structures. PhD dissertation, Southern Methodist University, Dallas, Texas, pp. 266
15. MATLAB and Statistics Toolbox Release R (2019a) The MathWorks, Inc., Natick, Massachusetts, United States
16. SeismoSignal v2022 Release-1 Build-50, Seismosoft Ltd. Retrieved from www.seismosoft.com
17. Iervolino I (2013) Probabilities and fallacies: why hazard maps cannot be validated by individual earthquakes. *Earthq Spectra* 29(3):1125–1136. <https://doi.org/10.1193/1.4000152>
18. Chen G (2023) Report on pulse-like ground motions in the Feb 2023 Turkey earthquakes. <https://doi.org/10.13140/RG.2.2.31375.25767>